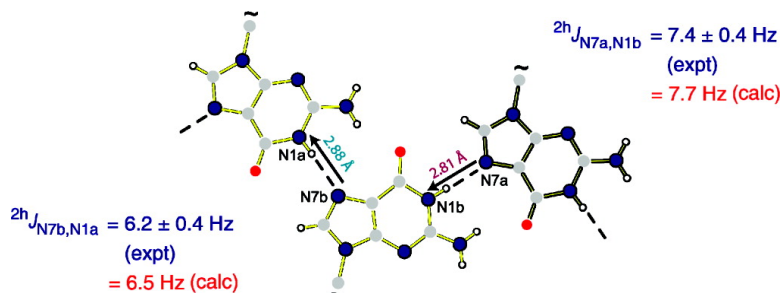Article

Density Functional Theory Calculations of Hydrogen-Bond-Mediated NMR *J* Coupling in the Solid State

Sia#n A. Joyce, Jonathan R. Yates, Chris J. Pickard, and Steven P. Brown

More About This Article

Additional resources and features associated with this article are available within the HTML version:

- Supporting Information
- Links to the 1 articles that cite this article, as of the time of this article download
- Access to high resolution figures
- Links to articles and content related to this article
- Copyright permission to reproduce figures and/or text from this article

View the Full Text HTML

Density Functional Theory Calculations of Hydrogen-Bond-Mediated NMR *J* Coupling in the Solid State

Siân A. Joyce,[†] Jonathan R. Yates,*,[‡] Chris J. Pickard,[§] and Steven P. Brown[||]

Tyndall National Institute, Lee Maltings, Prospect Row, Cork, Ireland, TCM Group, Cavendish Laboratory, University of Cambridge, 19 J. J. Thomson Avenue, Cambridge CB3 OHE, U.K., School of Physics and Astronomy, University of St. Andrews, North Haugh, St. Andrews KY16 9SS, U.K., and Department of Physics, University of Warwick, Coventry CV4 7AL, U.K.

Received January 18, 2008; E-mail: jry20@cam.ac.uk

Abstract: A recently developed method for calculating NMR *J* coupling in solid-state systems is applied to calculate hydrogen-bond-mediated $^{2h}J_{NN}$ couplings across intra- or intermolecular N−H···N hydrogen bonds in two 6-aminofulvene-1-aldimine derivatives and the ribbon structure formed by a deoxyguanosine derivative. Excellent quantitative agreement is observed between the calculated solid-state *J* couplings and those previously determined experimentally in two recent spin-echo magic-angle-spinning NMR studies (Brown, S. P.; et al. *Chem. Commun.* **2002**, 1852−1853 and Pham, T. N.; et al. *Phys. Chem. Chem. Phys.* **2007**, *9*, 3416−3423). For the 6-aminofulvene-1-aldimines, the differences in $^{2h}J_{NN}$ couplings in pyrrole and triazole derivatives are reproduced, while for the guanosine ribbons, an increase in $^{2h}J_{NN}$ is correlated with a decrease in the N−H···N hydrogen-bond distance. *J* couplings are additionally calculated for isolated molecules of the 6-aminofulvene-1-aldimines extracted from the crystal with and without further geometry optimization. Importantly, it is shown that experimentally observed differences between *J* couplings determined by solution- and solid-state NMR are not solely due to differences in geometry; long-range electrostatic effects of the crystal lattice are shown to be significant also. *J* couplings that are yet to be experimentally measured are calculated. Notably, $^{2h}J_{NO}$ couplings across N−H···O hydrogen bonds are found to be of a similar magnitude to $^{2h}J_{NN}$ couplings, suggesting that their utilization and quantitative determination should be experimentally feasible.

1. Introduction

The *J*-coupling mechanism is an essential component of many NMR experiments. The through-bond nature of the interaction is a powerful probe of molecular structures, allowing a unique insight into the connectivities of atoms. *J* coupling has recently received much attention as a measure of the presence and strength of hydrogen bonding, allowing the identification of the donor and acceptor atoms and the determination of hydrogen-bond geometries.[1] This interest in hydrogen-bond-mediated *J* couplings was largely prompted by the work of Dingley and Grzesiek,[2] who determined $^{2h}J_{NN}$ couplings in solution-state NMR. Since then, the use of $^{2h}J_{NN}$ HNN-COSY experiments has been established as an invaluable tool in understanding N−H···N hydrogen bonds.[3−5] The computational community has also been inspired by this advance, and the strong links between experiment and calculation have furthered the development of *J*-coupling methodology; in particular, there has been

much work on empirical relations between *J* coupling and the hydrogen-bond environment.[1,6,7] For example, $^{2h}J_{NN}$ couplings for hydrogen-bonded nucleic acid base pairs have been calculated by density functional theory (DFT) methods,[8−10] while smaller model hydrogen-bonded complexes have been investigated using DFT[11,12] and multiconfiguration self-consistent field (MCSCF)[13,14] calculations and extensively studied using the equation-of-motion−coupled-cluster singles and doubles (EOM−CCSD) method.[15−27] The size of the systems considered

[†] Tyndall National Institute.
[‡] University of Cambridge.
[§] University of St. Andrews.
[||] University of Warwick.
(1) Grzesiek, S.; Cordier, F.; Jaravine, V.; Barfield, M. *Prog. Nucl. Magn. Reson. Spectrosc.* **2004**, *45*, 275–300.
(2) Dingley, A. J.; Grzesiek, S. *J. Am. Chem. Soc.* **1998**, *120*, 8293–8297.
(3) Pervusin, K.; Ono, A.; Fernandez, C.; Szyperski, T.; Kainoso, M.; Wuthrich, K. *Proc. Natl. Acad. Sci. U.S.A.* **1998**, *95*, 14147–14151.
(4) Collin, D.; van Heijenoort, C.; Boiziau, C.; Toulme, J. J.; Guittet, E. *Nucleic Acids Res.* **2000**, *28*, 3386–3391.
(5) Cornish, P. V.; Giedroc, D. P.; Hennig, M. *J. Biomol. NMR* **2006**, *35*, 209–223.

(6) Alkorta, I.; Elguero, J. *Int. J. Mol. Sci.* **2003**, *4*, 64–92.
(7) Alkorta, I.; Elguero, J.; Denisov, G. S. *Magn. Reson. Chem.* **2008**, *46*, 599–624.
(8) Dingley, A. J.; Masse, J. E.; Peterson, R. D.; Barfield, M.; Feigon, J.; Grzesiek, S. *J. Am. Chem. Soc.* **1999**, *121*, 6019–6027.
(9) Scheurer, C.; Brüschweiler, R. *J. Am. Chem. Soc.* **1999**, *121*, 8661–8662.
(10) Barfield, M.; Dingley, A. J.; Feigon, J.; Grzesiek, S. *J. Am. Chem. Soc.* **2001**, *123*, 4014–4022.
(11) Benedict, H.; Shenderovich, I. G.; Malkina, O. L.; Malkin, V. G.; Denisov, G. S.; Golubev, N. S.; Limbach, H. H. *J. Am. Chem. Soc.* **2000**, *122*, 1979–1988.
(12) Van Mourik, T.; Dingley, A. J. *ChemPhysChem* **2007**, *8*, 288–296.
(13) Pecul, M.; Leszczynski, J.; Sadlej, J. *J. Phys. Chem. A* **2000**, *104*, 8105–8113.
(14) Bryce, D. L.; Wasylischen, R. E. *J. Biomol. NMR* **2001**, *19*, 371–375.
(15) Del Bene, J. E.; Perera, A. A.; Bartlett, R. J. *J. Am. Chem. Soc.* **2000**, *122*, 3560–3561.
(16) Del Bene, J. E.; Bartlett, R. J. *J. Am. Chem. Soc.* **2000**, *122*, 10480–10481.
(17) Del Bene, J. E.; Perera, A. A.; Bartlett, R. J. *J. Phys. Chem. A* **2001**, *105*, 930–934.

in these calculations is relatively small: in the EOM−CCSD studies, the largest complex studied (pyridine−H⁺···pyridine) had 23 atoms,[27] while the largest TAT nucleic acid trimer studied by DFT in ref 10 had 45 atoms. Nevertheless, these calculations have identified trends that support and provide additional insight into experimental data, notably the establishment of a clear correlation between an increased $^{2h}J_{NN}$ coupling constant and a decreased N···N hydrogen-bonding distance. For example, Figure 2 in ref 27 presents calculations for 40 model protonated hydrogen-bonded dimers: large $^{2h}J_{NN}$ values (20−40 Hz) were calculated for hydrogen-bonded complexes with complete or significant proton-shared character (i.e., N···H···N), while for traditional hydrogen bonds (i.e., NH···N), $^{2h}J_{NN}$ values between 15 and 5 Hz, corresponding to N···N distances increasing from 2.7 to 3.2 Å, were calculated.

While solution-state NMR has a long history of both exploiting and measuring *J* coupling, in solid-state NMR, the line widths of ordinary 1D spectra are broadened by anisotropic interactions and the multiplet splittings of the spectral peaks are usually obscured. However, through the use of spin-echo magic-angle-spinning (MAS)-based experiments, the determination of solid-state *J* couplings has become more routine in both organic[28−36] and inorganic[37−45] systems. To complement

and support these advances in experimental technique, we have recently developed an all-electron first-principles method for calculating NMR *J* coupling in solid-state systems.[46] This approach is DFT-based and uses plane waves and periodic boundary conditions within the plane-wave pseudopotential framework.[47] The use of plane waves in combination with periodic boundary conditions enables us to utilize the translational symmetry inherent in crystal structures and implicitly include long-range electrostatic effects of the crystal lattice.

In this work, we have applied our solid-state method to calculate *J* couplings, in particular, the ¹⁵N−¹⁵N couplings across intra- and intermolecular hydrogen bonds, for two molecular crystals, the 6-aminofulvene-1-aldimines[28,48−51] and a deoxyguanosine derivative,[36,43,52] where the individual molecules contain between 33 and 45 atoms each. Excellent agreement is observed between the calculated *J* couplings and those determined experimentally by the spin-echo MAS NMR approach[28,36] for the solid-state hydrogen-bonded systems considered here, which are significantly larger than the model systems that have been investigated in the quantum-chemical studies published to date (see above). Moreover, the inherent solid-state nature of our method avoids the investigation of what constitutes an appropriate cluster of individual molecules for modeling the solid state, which is required in the case of traditional quantum-chemical methods. Furthermore, we emphasize the great advantage of comparing experiment and calculation in the solid state as opposed to the established approach of comparing solution-state experimentals with gas-phase calculations: there is no complication from solvent effects and hence no need to consider solvent effects in the calculations. For the 6-aminofulevene-1-aldimines, *J* couplings are additionally calculated for isolated molecules extracted from the crystal with and without further structural optimization. Importantly, it is shown that experimentally observed differences between *J* couplings determined by solution- and solid-state NMR are not solely due to differences in geometry; long-range electrostatic effects of the crystal lattice are shown to be significant also.

2. Computational Details

We followed the same procedure when calculating the *J* coupling for each system. A fully unconstrained geometry optimization of all of the atomic positions with fixed cell parameters was first performed, starting from the published crystal structure. We then used the optimized structure in the calculation of the *J* coupling. All of the calculations were performed using the DFT code CASTEP,[53] in which the wave functions and charge density are

(18) Del Bene, J. E.; Perera, A. A.; Bartlett, R. J. *Magn. Reson. Chem.* **2001**, *39*, S109–S119.
(19) Jordan, M. J. T.; Toh, J. S. S.; Del Bene, J. E. *Chem. Phys. Lett.* **2001**, *346*, 288–292.
(20) Toh, J. S. S.; Jordan, M. J. T.; Husowitz, B. C.; Del Bene, J. E. *J. Phys. Chem. A* **2001**, *105*, 10906–10914.
(21) Del Bene, J. E.; Elguero, J. *Magn. Reson. Chem.* **2004**, *42*, 421–423.
(22) Alkorta, I.; Elguero, J.; Mo, O.; Yanez, M.; Del Bene, J. E. *Mol. Phys.* **2004**, *102*, 2563–2574.
(23) Del Bene, J. E.; Elguero, J. *J. Am. Chem. Soc.* **2004**, *126*, 15624–15631.
(24) Del Bene, J. E.; Elguero, J. *J. Phys. Chem. A* **2004**, *108*, 11762–11767.
(25) Del Bene, J. E.; Elguero, J.; Alkorta, I.; Mó, O.; Yanez, M. *J. Phys. Chem. A* **2005**, *109*, 2350–2355.
(26) Alkorta, I.; Elguero, J.; Mó, O.; Yanez, M.; Del Bene, J. E. *Chem. Phys. Lett.* **2005**, *411*, 411–415.
(27) Del Bene, J. E.; Elguero, J. *J. Phys. Chem. A* **2006**, *110*, 7496–7502.
(28) Brown, S. P.; Perez-Torralba, M.; Sanz, D.; Claramunt, R. M.; Emsley, L. *Chem. Commun.* **2002**, 1852–1853.
(29) De Paepe, G.; Giraud, N.; Lesage, A.; Hodgkinson, P.; Bockmann, A.; Emsley, L. *J. Am. Chem. Soc.* **2003**, *125*, 13938–13939.
(30) Sakellariou, D.; Brown, S. P.; Lesage, A.; Hediger, S.; Bardet, M.; Meriles, C. A.; Pines, A.; Emsley, L. *J. Am. Chem. Soc.* **2003**, *125*, 4376–4380.
(31) Duma, L.; Lai, W. C.; Carravetta, M.; Emsley, L.; Brown, S. P.; Levitt, M. H. *ChemPhysChem* **2004**, *5*, 815–833.
(32) Brown, S. P.; Emsley, L. *J. Magn. Reson.* **2004**, *171*, 43–47.
(33) Lai, W. C. *J. Am. Chem. Soc.* **2006**, *128*, 3878–3879.
(34) Cadars, S.; Lesage, A.; Hedin, N.; Chmelka, B. F.; Emsley, L. *J. Phys. Chem. B* **2006**, *110*, 16982–16991.
(35) Cadars, S.; Lesage, A.; Trierweiler, M.; Heux, L.; Emsley, L. *Phys. Chem. Chem. Phys.* **2007**, *9*, 92–103.
(36) Pham, T. N.; Griffin, J. M.; Masiero, S.; Lena, S.; Gottarelli, G.; Hodgkinson, P.; Filip, C.; Brown, S. P. *Phys. Chem. Chem. Phys.* **2007**, *9*, 3416–3423.
(37) Kubo, A.; McDowell, C. A. *J. Chem. Phys.* **1990**, *92*, 7156–7170.
(38) Challoner, R.; Nakai, T.; McDowell, C. A. *J. Chem. Phys.* **1991**, *94*, 7038–7045.
(39) Wu, G.; Wasylishen, R. E. *Inorg. Chem.* **1992**, *31*, 145–148.
(40) Fayon, F.; King, I. J.; Harris, R. K.; Gover, R. K. B.; Evans, J. S. O.; Massiot, D. *Chem. Mater.* **2003**, *15*, 2234–2239.
(41) Fayon, F.; King, I. J.; Harris, R. K.; Evans, J. S. O.; Massiot, D. *C. R. Chim.* **2004**, *7*, 351–361.
(42) Eichele, K.; Nachtigal, C.; Jung, S.; Mayer, H. A.; Lindner, E.; Strobele, M. *Magn. Reson. Chem.* **2004**, *42*, 807–813.
(43) Pham, T. N.; Masiero, S.; Gottarelli, G.; Brown, S. P. *J. Am. Chem. Soc.* **2005**, *127*, 16018–16019.
(44) de Araujo, C. C.; Strojek, W.; Zhang, L.; Eckert, H.; Poirier, G.; Ribeiro, S. J. L.; Messaddeq, Y. *J. Mater. Chem.* **2006**, *16*, 3277–3284.

(45) Foucault, H. M.; Bryce, D. L.; Fogg, D. E. *Inorg. Chem.* **2006**, *45*, 10293–10299.
(46) Joyce, S. A.; Yates, J. R.; Pickard, C. J.; Mauri, F. *J. Chem. Phys.* **2007**, *127*, 204107.
(47) Payne, M. C.; Teter, M. P.; Allen, D. C.; Arias, T. A.; Joannopoulos, J. D. *Rev. Mod. Phys.* **1992**, *64*, 1045–1097.
(48) Claramunt, R. M.; Sanz, D.; Alarcón, S. H.; Pérez-Torralba, M.; Elguero, J.; Foces-Foces, C.; Pietrzak, M.; Langer, U.; Limbach, H. *Angew. Chem., Int. Ed.* **2001**, *40*, 420–423.
(49) Pietrzak, M.; Limbach, H.; Pérez-Torralba, M.; Sanz, D.; Claramunt, R. M.; Elguero, J. *Magn. Reson. Chem.* **2001**, *39*, S100–S108.
(50) Brown, S. P.; Perez-Torralba, M.; Sanz, D.; Claramunt, R. M.; Emsley, L. *J. Am. Chem. Soc.* **2002**, *124*, 1152–1153.
(51) Sanz, D.; Pérez-Torralba, M.; Alarcón, S. H.; Claramunt, R. M.; Foces-Foces, C.; Elguero, J. *J. Org. Chem.* **2002**, *67*, 1462–1471.
(52) Giorgi, T.; Grepioni, F.; Manet, I.; Mariani, P.; Masiero, S.; Mezzina, E.; Pieraccini, S.; Saturni, L.; Spada, G. P.; Gottarelli, G. *Chem.−Eur. J.* **2002**, *8*, 2143–2152.
(53) Clark, S. J.; Segall, M. D.; Pickard, C. J.; Probert, M. J.; Hasnip, P. J.; Refson, K.; Payne, M. C. *Z. Kristallogr.* **2005**, *220*, 567–570.
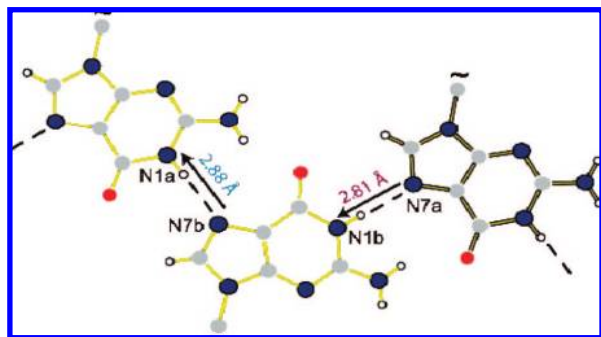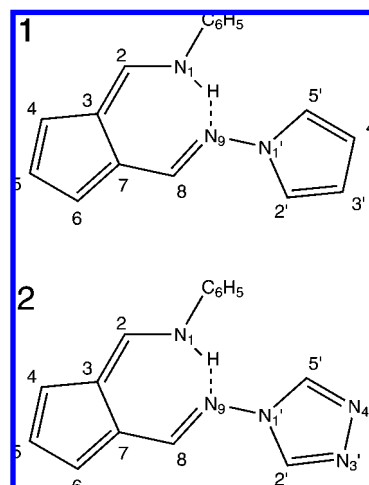
Figure 1. Intermolecular hydrogen bonding in **3**: a view of the crystal structure (after geometry optimization) indicating the two symmetrically distinct molecules in the unit cell. Nitrogen, oxygen, carbon, and hydrogen atoms are represented as blue, red, gray, and white circles, respectively.

expanded in a plane-wave basis. Troullier–Martins[54] norm-conserving pseudopotentials were used to represent the interaction of the valence electrons with the nucleus and the core electrons, thereby greatly enhancing the computational efficiency of the approach. The exchange and correlation effects were approximated by the generalized gradient approximation of Perdew, Burke, and Ernzerhof.[55] We used a maximum grid spacing of $0.04\ \text{Å}^{-1}$ to sample the Brillouin zone. It was straightforward to numerically converge the calculated *J* couplings with the size of the basis set used in our calculations; a plane-wave basis represents a uniform sampling of space, and the quality of the basis is controlled by a single parameter, namely, the maximum-energy plane wave included in the basis. We used plane waves up to an energy of 80 rydberg, which gave convergence within 0.1 Hz for the *J* couplings reported here.

The isotropic *J* coupling was obtained from density functional perturbation theory, and the projector-augmented wave (PAW) technique[56] was used to obtain *J* couplings with all-electron accuracy. The *J* couplings were computed as the sum of all four of the Ramsey terms.[57] The details of the method are outlined in ref 46, and it is related to the GIPAW approach[58] for calculating chemical shifts. It is a fully solid-state theory in which the *J* coupling is treated as a perturbation between the magnetic moment of a chosen atom and those of all of the remaining atoms in the system. This perturbation breaks the translational symmetry of the crystal, requiring us to choose a simulation cell of sufficient size to inhibit the interaction of periodically repeated images of the perturbing site. The localized nature of the *J*-coupling interaction means that the primitive crystallographic cell is often large enough to give converged results; however, in some cases we found it necessary to consider a larger simulation cell containing two or more primitive cells. *J* couplings in molecular systems can be calculated using a vacuum-supercell technique.

2.1. 6-Aminofulvene-1-aldimines. The crystal structures for the pyrrole (**1**) and triazole (**2**) 6-aminofulvene-1-aldimine derivatives[48,51] were obtained from the Chemical Database Service (CDS)[59] (reference codes IFANEI and WOWLID, respectively). The pyrrole structure has eight symmetry-related molecules per unit cell and a total of 280 atoms. The triazole structure is smaller, with four symmetry-related molecules per unit cell and a total of 132 atoms. The pyrrole and triazole derivatives both exhibit *intramolecular* hydrogen bonding within a seven-membered ring. We note that the publication of the experimental determination of hydrogen-bond-mediated *J* couplings for these and other related compounds in the solution state[48,49,51] was an impetus for quantum-chemical studies
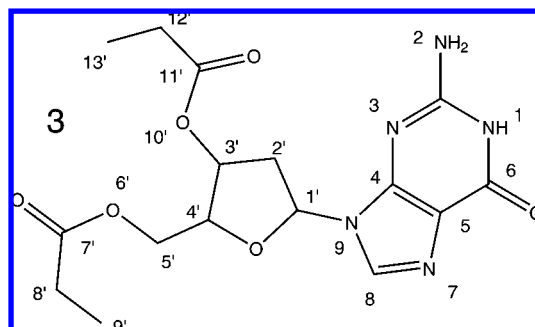
examining differences in intramolecular hydrogen bonding in saturated and unsaturated analogues.[22,26] We emphasize that the real systems considered here are much bigger than the 11- or 13-atom model diaza derivatives of propanediol studied by Alkorta et al.[22,26]

All of the *J* couplings between the N_9 nitrogen atom and the other atoms in each 6-aminofulvene-1-aldimine structure were calculated. For both derivatives, the *J* couplings were found to be converged within the primitive crystallographic cell. These calculations were performed on eight 64-bit, dual-core AMD processors. In total, the ground-state and *J*-coupling calculations for the optimized pyrrole and triazole systems took approximately 14 and 8 h, respectively.

We used two different approaches to interpret the experimentally observed differences between *J* couplings determined by solution- and solid-state NMR.[28] In each approach, a molecule was taken from each of the crystal structures. In the first case, a fully unconstrained geometry optimization was carried out, and in the second, the crystalline geometry was preserved. In both instances, the isolated molecule was placed in a $20 \times 20 \times 20$ Å vacuum supercell, and the calculations were performed at a single **k** point. All of the other parameters in the calculation remained the same as above. The *J*-coupling calculation was performed by considering the coupling between the N_9 nitrogen and all of the other atoms.

2.2. Guanosine Ribbons. The structure of the short-chained deoxyguanosine[52] derivative (**3**) was obtained from the CDS (reference code MOFBUE). There are two inequivalent molecules (labeled a and b in this paper) per unit cell and a total of 96 atoms. The exhibited *intermolecular* hydrogen bonding is shown schematically in Figure 1.

To calculate the *J* coupling, a $2 \times 1 \times 1$ supercell of the crystallographic unit cell was constructed. This ensured that the *J* coupling was fully converged within the supercell. The *J* coupling was calculated for both molecules in the unit cell. Each calculation was performed on eight 64-bit, dual-core AMD processors and took

(54) Troullier, N.; Martins, J. L. *Phys. Rev. B* **1991**, *43*, 1993–2006.
(55) Perdew, J. P.; Burke, K.; Ernzerhof, M. *Phys. Rev. Lett.* **1996**, *77*, 3865–3868.
(56) Blöchl, P. E. *Phys. Rev. B* **1994**, *50*, 17953–17979.
(57) Ramsey, N. F. *Phys. Rev.* **1953**, *91*, 303–307.
(58) Pickard, C. J.; Mauri, F. *Phys. Rev. B* **2001**, *63*, 245101.
(59) Fletcher, D. A.; McMeeking, R. F.; Parkin, D. *J. Chem. Inf. Comput. Sci.* **1996**, *36*, 746–749.

Table 1. Calculated and Experimental $^{2h}J_{N_9N_1}$ and $^1J_{N_9N_1'}$ Couplings (Hz) for the Pyrrole (**1**) and Triazole (**2**) 6-Aminofulvene-1-aldimine Derivatives

		pyrrole (**1**)		triazole (**2**)		$|J_{pyrrole}| - |J_{triazole}|$	
		$^{2h}J_{N_9N_1}$	$^1J_{N_9N_1'}$	$^{2h}J_{N_9N_1}$	$^1J_{N_9N_1'}$	$^{2h}J_{N_9N_1}$	$^1J_{N_9N_1'}$
solid-state	calcd	8.1	−9.8	7.4	−11.4	0.7	−1.6
	exptl[a]	8.0 ± 0.3	10.2 ± 0.4	7.2 ± 0.1	12.0 ± 0.1	0.8	−1.8
solution-state	calcd (rel. mol.)[b]	9.8	−9.4	9.5	−10.8	0.3	−1.4
	exptl[c]	9.0	10.3	8.6	11.8	0.4	−1.5

[a] Data from ref 28. [b] The label "rel. mol." refers to the fully relaxed structure of the isolated molecule. [c] Data from refs 48 and 51.

approximately 10 h to complete. We also obtained the ^{15}N chemical shifts using the GIPAW approach. Further computational details can be found in the Supporting Information.

3. Results and Discussion

3.1. Comparison with Experiment. Reference 50 presented a 2D MAS INADEQUATE[60−63] spectrum of **2** that revealed double-quantum (DQ) peaks for N_9 with both N_1' and N_1, the latter constituting the first experimental observation of a hydrogen-bond-mediated J coupling in the solid state. The $^1J_{N_9N_1'}$ and $^{2h}J_{N_9N_1}$ couplings have been determined for both **1** and **2** in both solution[48,51] and the solid-state, the latter using spin-echo MAS techniques.[28] In this work, we have calculated the $^{15}N_9−X$ J couplings for **1** and **2** in their periodic crystal structures and as isolated molecules.

Table 1 compares the calculated $^1J_{N_9N_1'}$ and $^{2h}J_{N_9N_1}$ couplings for the crystal structures of **1** and **2** and the experimental solid-state NMR results from ref 28. It is clear that the computed couplings are in excellent agreement with experiment. Both the directly bonded and hydrogen-bond-mediated couplings in the pyrrole and triazole derivatives are accurately reproduced. We have also identified the signs of the couplings, as this property is not determined from the experimental spin-echo-based approaches, where a $\cos(\pi J\tau)$ modulation is observed. The $^{2h}J_{NN}$ couplings are positive, as is to be expected for a traditional X−H···Y hydrogen bond in which the magnetogyric ratios of X and Y have the same sign.[21,24]

Table 1 also presents a comparison of the couplings calculated for the fully relaxed, isolated molecules with the experimentally determined solution-state values from refs 48 and 51. As these calculations were performed for an isolated molecule in vacuum, they do not account for the effects of solvation, and we therefore expect the results to be less accurate than the solid-state values. In this context, we note that the importance of solvent effects on solution-state J couplings has been discussed in recent quantum-chemical studies.[64,65] Nevertheless, the results in Table 1 are in reasonable agreement with experiment. Notably, although the absolute differences between the solution- and solid-state values are overestimated with respect to experiment, the calculations also show a decrease in magnitude of the hydrogen-bond-mediated J couplings in going from the solution- to the solid-state systems, indicating that the hydrogen bond in the solid state is weaker than that in solution, as previously noted

Table 2. Calculated and Measured Solid-State $^{2h}J_{NN}$ Couplings (Hz) and ^{15}N Chemical Shifts (ppm) for the $N_1−H···N_7$ Intermolecular Hydrogen Bonds in the Deoxyguanosine Ribbons Formed by **3**

		$^{2h}J_{N_jN_k}$	$\delta(^{15}N_j)$	$\delta(^{15}N_k)$	$|N_j···N_k|^a$
$N_{1a}−H···N_{7b}$	calcd	6.5	−234.5	−137.9	2.88
	exptl[b]	6.2 ± 0.4	−231.9	−139.0	2.88
$N_{1b}−H···N_{7a}$	calcd	7.7	−231.6	−143.9	2.81
	exptl[b]	7.4 ± 0.4	−230.4	−143.1	2.81

[a] $|N_j···N_k|$ refers to the $N_j···N_k$ hydrogen-bond distance (Å) for the optimized geometry. [b] Data from ref 36.

in ref 28 (differences between solid- and solution-state J couplings are discussed further in Section 3.2.) Table 1 also considers the changes in the $^1J_{N_9N_1'}$ and $^{2h}J_{N_9N_1}$ couplings due to the change in the N_9 substituent from pyrrole to triazole. The calculations accurately reproduce these changes for both the solid- and solution-state experiments. The previously mentioned error in the calculated solution values is dramatically reduced because the solvent effects have been implicitly eliminated by the molecule-to-molecule comparison.

J couplings were also calculated for the short-chained deoxyguanosine derivative $dG(C_3)_2$ (**3**). Guanine has featured strongly in solution- and solid-state explorations of hydrogen bonding and hydrogen-bonded systems and has been an important component in understanding N−H···N bonding[66−68] and hydrogen-bond cooperativity.[69] As shown in Figure 1, the crystal structure reveals that **3** self-assembles into a ribbon-like structure via intermolecular N−H···N hydrogen bonds; specifically, there are two distinct molecules in the asymmetric unit cell with two different N−H···N hydrogen-bond lengths. An ^{15}N-refocused INADEQUATE[70,71] solid-state NMR spectrum of **3** revealed DQ correlations corresponding to the intramolecular $^2J_{NN}$ couplings between N_1 and N_2, N_2 and N_3, and N_3 and N_9 as well as the intermolecular hydrogen-bond-mediated $^{2h}J_{NN}$ coupling between N_1 and N_7.[36] The $^{2h}J_{N_1N_7}$, $^2J_{N_2N_3}$, and $^2J_{N_3N_9}$ couplings have been quantitatively determined using solid-state ^{15}N spin-echo MAS experiments.[36]

The experimentally determined $^{2h}J_{NN}$ couplings for the two distinct $N_1−H···N_7$ hydrogen bonds as well as the four ^{15}N chemical shifts are listed in Table 2 along with the calculated solid-state couplings and chemical shifts. Excellent agreement between calculation and experiment is observed. The calculated

(60) Early, T. A.; John, B. K.; Johnson, L. F. *J. Magn. Reson.* **1987**, *75*, 134–138.
(61) Benn, R.; Grondey, H.; Brevard, C.; Pagelot, A. *J. Chem. Soc., Chem. Commun.* **1988**, 102–103.
(62) Fyfe, C. A.; Feng, Y.; Gies, H.; Grondey, H.; Kokotailo, G. T. *J. Am. Chem. Soc.* **1990**, *112*, 3264–3270.
(63) Lesage, A.; Auger, C.; Caldarelli, S.; Emsley, L. *J. Am. Chem. Soc.* **1997**, *119*, 7867–7868.
(64) Sahakyan, A. B.; Shahkhatuni, A. A.; Shahkhatuni, A. G.; Panosyan, H. A. *Magn. Reson. Chem.* **2008**, *46*, 63–68.
(65) Del Bene, J. E.; Elguero, J. *Magn. Reson. Chem.* **2007**, *45*, 484–489.

(66) Sychrovský, V.; Schneider, B.; Hobza, P.; Židek, L.; Sklenář, V. *Phys. Chem. Chem. Phys.* **2003**, *5*, 734–739.
(67) Van Mourik, T.; Dingley, A. J. *Chem.—Eur. J.* **2005**, *11*, 6064–6079.
(68) Van Mourik, T. *J. Chem. Phys.* **2006**, *125*, 191101.
(69) Van Mourik, T.; Dingley, A. J. *J. Phys. Chem. A* **2007**, *111*, 11350–11358.
(70) Lesage, A.; Bardet, M.; Emsley, L. *J. Am. Chem. Soc.* **1999**, *121*, 10987–10993.
(71) Fayon, F.; Massiot, D.; Levitt, M. H.; Titman, J. J.; Gregory, D. H.; Duma, L.; Emsley, L.; Brown, S. P. *J. Chem. Phys.* **2005**, *122*, 194313.

Table 3. Calculated *J* Couplings (Hz) and Geometric Parameters for the N−H···N Hydrogen Bonds in Compounds **1**, **2**, and **3** Together with Experimental Solution-State *J* Couplings

		X, Y	$^1J_{XH}$	$^{1h}J_{YH}$	|X−H|[c]	|Y···H|[d]	$\alpha_{X-H···Y}$[e]
1	calcd (solid-state)	N₁, N₉	−76.0	1.42	1.05	1.82	156.2
	calcd (rel. mol.)		−74.1	1.15	1.06	1.74	158.1
	exptl (solution-state)[a]			88.2	4.0		
2	calcd (solid-state)	N₁, N₉	−76.7	1.72	1.05	1.85	154.6
	calcd (rel. mol.)		−74.3	1.54	1.05	1.75	158.1
	exptl (solution-state)[b]			88.6	4.4		
3	calcd (solid-state)	N₁ₐ, N₇ᵦ	−73.6	0.60	1.06	1.82	177.8
	calcd (solid-state)	N₁ᵦ, N₇ₐ	−75.4	0.71	1.07	1.74	178.8

[a] Data from ref 48. [b] Data from ref 51. [c] |X−H| refers to the X−H bond length (Å). [d] |Y···H| refers to the Y···H hydrogen-bond distance (Å). [e] $\alpha_{X-H···Y}$ refers to the X−H···Y hydrogen-bond angle (deg).

chemical shifts clearly assign the measured $^{2h}J_{NN}$ couplings to the two distinct molecules in the unit cell. The calculated *J* couplings are within experimental error and confirm the expectation outlined in ref 36 that the larger *J* coupling corresponds to the shorter N−N bond length; this is in agreement with previous quantum-chemical studies on smaller model systems.[8−10,27]

For completeness, Table 3 lists the $^1J_{NH}$ and $^{1h}J_{NH}$ coupling constants calculated for the three systems. The calculated $^1J_{NH}$ and $^{1h}J_{NH}$ couplings are negative and positive, respectively, as expected for a traditional X−H···Y hydrogen bond in which the magnetogyric ratio of X (i.e., ¹⁵N) is negative.[24] We note that the signs of the $^1J_{XH}$, $^{1h}J_{YH}$, and $^{2h}J_{XX}$ coupling constants have been explained by an NMR triplet wave functional model.[21,72] From a comparison of the calculated coupling constants for **1** and **2**, it is apparent that both $^1J_{NH}$ and $^{1h}J_{NH}$ have larger magnitudes for **2**, where the hydrogen bond is weaker, as evidenced by the longer N···N and N···H distances. These observations are consistent with the trends observed in previous quantum-chemical studies of small model dimers.[23,24] To date, there has been no experimental solid-state NMR determination of the $^1J_{NH}$ and $^{1h}J_{NH}$ coupling constants for any of the three compounds; the determination of *J* couplings involving protons in the solid state is complicated by the requirement that homonuclear ¹H decoupling techniques be applied during the heteronuclear spin echo, and such decoupling techniques lead to a scaling of the *J* evolution, with the scaling itself being dependent on the experimental parameters. From a comparison of the calculated $^1J_{NH}$ and $^{1h}J_{NH}$ values for the relaxed molecules to the solution-state NMR data for **1** and **2**,[48,51] it is evident that the calculated coupling constants are smaller in magnitude than the experimental data. As in the above discussion of $^{2h}J_{NN}$ (see Table 1), we note here the importance of solvation effects and that care must be taken when comparing the results of gas-phase calculations and solution-state NMR experiments.

As described above, the $^2J_{N_2N_3}$ and $^2J_{N_3N_9}$ two-bond intramolecular couplings were determined experimentally for **3** (ref 36). However, there was insufficient resolution between the N₉ and N₃ resonances from the two independent molecules to permit a separate determination of the $^2J_{NN}$ couplings for each distinct molecule (the spin-echo experiments in ref 36 were performed at an ¹⁵N Larmor frequency of 30 MHz, with the full-width at half-maximum line widths exceeding 1 ppm). We present the calculated intramolecular N−N couplings and

(72) Del Bene, J. E.; Elguero, J. *Chem. Phys. Lett.* **2003**, *382*, 100−105.

Table 4. Calculated and Measured Solid-State $^2J_{NN}$ Couplings (Hz) and Corresponding ¹⁵N Chemical Shifts (ppm) for **3**[a]

Nⱼ−Nₖ		J	δ(¹⁵Nⱼ)	δ(¹⁵Nₖ)
N₂ₐ−N₃ₐ	calcd	5.4	−306.5	−216.4
	exptl[b]	6.6 ± 0.7	−305.5	−217.7
N₂ᵦ−N₃ᵦ	calcd	5.7	−305.5	−212.7
	exptl[b]	6.6 ± 0.7	−305.5	−215.8
N₃ₐ−N₉ₐ	calcd	4.4	−216.4	−211.6
	exptl[b]	4.3 ± 0.2	−217.7	−210.2
N₃ᵦ−N₉ᵦ	calcd	4.2	−212.7	−209.4
	exptl[b]	4.3 ± 0.2	−215.8	−210.2

[a] The labels a and b denote the two distinct molecules of **3** in the crystallographic unit cell and refer to molecules 1 and 2, respectively, in ref 52. [b] Only one *J* coupling was determined experimentally because of insufficient resolution of the ¹⁵N resonances.

¹⁵N chemical shifts for N₂, N₃, and N₉ in Table 4. Again, we see that the calculated values agree very well with experiment. The calculated N₃−N₉ *J* couplings are within experimental error, while the N₂−N₃ values are slightly underestimated, although the larger experimental error associated with the determination of the N₂−N₃ *J* couplings from fitting of the N₃ experimental spin-echo data to a modulation by the N₂−N₃ and N₃−N₉ *J* couplings should be noted.[36]

3.2. Solid-State Effects. The 6-aminofulvene-1-aldimines offer a valuable opportunity to understand the extent to which the crystal lattice affects *J* coupling in the solid state. Our fully solid-state method enables us to make a quantitative estimate of the role of these long-range electrostatic interactions. To this end, in addition to calculations for the full solid-state structures, we considered two model systems. In the first model, a single molecule was taken from the fully relaxed crystal structure, and no further geometry optimization was performed on it. This means that the *J* coupling was calculated using the same geometry as in the solid-state structure but without the long-range electrostatic interactions which arise from the contact and packing interactions present in the molecular crystal. If the *J* coupling is a truly local interaction, these electrostatic interactions should have a negligible effect. We refer to this model as the constrained molecular (con. mol.) model. In the second scheme, to which Section 3.1 refers, an isolated molecule was obtained from the crystal structure and then fully relaxed in a vacuum supercell. We expect this model to correspond most closely to the molecule in the solution state. This model is called the relaxed molecular (rel. mol.) model. We note that neither of these two models accounts for solvation effects, and consequently, we do not expect to fully understand the experimentally observed difference between the solution and solid states. However, by comparing the values calculated in the two models, we can isolate and estimate the contributions to the solid-state *J* couplings that may arise from local structural effects and crystal-lattice interactions.

The results of these calculations are given in Table 5, where the differences between the solid-state and con. mol. values are labeled "electrostatic" and those between the rel. mol. and con. mol. values are labeled "structural". For both **1** and **2**, the difference between the $^1J_{N_9N_1'}$ couplings for the constrained and relaxed structures is small. This is to be expected, as there is essentially no difference between the N₉−N₁′ bond lengths of these models, as shown in Table 6. However, for both compounds there is an increase in the magnitude of the coupling upon moving from the con. mol. system to the full crystal structure, which we conclude must be due to long-range electrostatic effects.

Table 5. $^{2h}J_{N_9N_1}$ and $^1J_{N_9N_1'}$ Couplings (Hz) for **1** and **2** Calculated for the Solid-State and Isolated Molecules with and without Further Geometry Optimization

	pyrrole (**1**)		triazole (**2**)	
	$^{2h}J_{N_9N_1}$	$^1J_{N_9N_1'}$	$^{2h}J_{N_9N_1}$	$^1J_{N_9N_1'}$
rel. mol.[a]	9.8	−9.4	9.5	−10.8
con. mol.[b]	8.6	−9.4	8.0	−10.7
structural[c]	1.2	0.0	1.5	0.1
solid	8.1	−9.8	7.4	−11.4
electrostatic[d]	−0.5	0.4	−0.6	0.7

[a] For the model involving an isolated, fully relaxed molecule. [b] For the model involving a constrained molecule taken from the relaxed crystal structure without further geometry optimization. [c] |J(rel. mol.)| − |J(con. mol.)|. [d] |J(solid)| − |J(con. mol.)|.

Table 6. Bond Lengths (Å) for Isolated **1** and **2** Molecules with and without Further Geometry Optimization

	pyrrole (**1**)		triazole (**2**)	
	N_9—N_1	N_9—N_1'	N_9—N_1	N_9—N_1'
rel. mol.	2.75	1.38	2.75	1.39
con. mol.	2.81	1.40	2.83	1.39

The situation is more complex for the $^{2h}J_{N_9N_1}$ couplings. The N_9—N_1 bond lengths are approximately 0.07 Å shorter in the relaxed molecule than in the con. mol. structure (Table 6). As noted above, several previous quantum-chemical studies[9,10,15,16,27] have concluded that $^{2h}J_{N_j}$–H···N_k increases with decreasing N_j···N_k distance, and we indeed observe increases in the $^{2h}J_{N_9N_1}$ couplings (1.2 Hz for pyrrole, 1.5 Hz for triazole) in going from the constrained to the relaxed structures. We also note from Table 3 that there are corresponding increases in the N_1—H···N_9 bond angles. For both **1** and **2**, we observe a decrease of ∼0.5 Hz in the magnitude of the coupling on moving from the con. mol. system to the full crystal structure, which is similar to the change in the magnitude of the $^1J_{N_9N_1'}$ couplings.

The average difference between the four measured solid-state J couplings in **1** and **2** and the values computed using the full crystal structure is 0.3 Hz, which is comparable to the experimental error. The average difference rises to 0.9 Hz when the calculations for the con. mol. model are compared to the experimental solid-state J couplings (Tables 1 and 4). This shows that a computational approach that includes the electrostatic effects of the crystal lattice is essential for the accurate prediction of J couplings in solid-state systems, i.e., it is not sufficient to consider only the changes in the geometries of the individual molecules due to crystal packing. Notably, the changes of ∼0.5 Hz in both $^{2h}J_{N_9N_1}$ and $^1J_{N_9N_1'}$ ascribed to electrostatic effects in Table 5 constitute a non-negligible portion of the total solid-state coupling. The importance of both geometry changes and electrostatic effects has previously been noted in connection with the effect of the solvent on solution-state J couplings.[64,65] In conclusion, while J coupling is a localized interaction, it is nevertheless affected by changes to the charge density, which are both structural and electrostatic in nature.

3.3. Predicted J Couplings in Guanosine. Section 3.1 has demonstrated the excellent agreement between our calculated J couplings and experimentally determined values. In this section, we present calculated J couplings for the deoxyguanosine derivative that have not yet been experimentally measured. Of particular interest is the calculation of J couplings

Table 7. Calculated Solid-State ^{17}O and ^{15}N–^{15}N J Couplings (Hz) for **3**[a]

molecule a	calcd value	molecule b	calcd value
	^{17}O J Couplings		
$^{2h}J_{O_{6a}N_{2b}}$	5.7	$^{2h}J_{O_{6b}N_{2a}}$	5.3
$^1J_{O_{6a}C_{1a}}$	22.0	$^1J_{O_{6b}C_{1b}}$	22.4
$^2J_{O_{6a}C_{4a}}$	−1.7	$^2J_{O_{6b}C_{4b}}$	−1.7
	^{15}N–^{15}N J Couplings		
$^2J_{N_{1a}N_{2a}}$	2.4	$^2J_{N_{1b}N_{2b}}$	2.3
$^2J_{N_{1a}N_{3a}}$	−1.1	$^2J_{N_{1b}N_{3b}}$	−1.1
$^2J_{N_{7a}N_{9a}}$	−1.2	$^2J_{N_{7b}N_{9b}}$	−1.3

[a] The labels a and b denote the two distinct molecules of **3** in the crystallographic unit cell and refer to molecules 1 and 2, respectively, in ref 52.

involving the only NMR-active oxygen isotope, the $I = {}^5/_2$ nucleus ^{17}O. There have been very few reports of the determination of J couplings involving ^{17}O. This is due to the quadrupolar interaction, which causes fast relaxation in solution and anisotropic broadening in the solid-state. A recent solid-state NMR example is the determination of a $^1J_{OP}$ value of 161 ± 2 Hz for OPPh$_3$ by MAS[73] and subsequently DOR.[74] Iuga et al.[75] have also recently presented an ^{17}O–^{27}Al correlation experiment that uses $^1J_{OAl}$ couplings, although the couplings were not quantitatively determined. We are not aware of any reports of the experimental determination of a hydrogen-bond-mediated $^{2h}J_{ON}$ coupling in solution or the solid state, in spite of the great importance of O···H–N hydrogen bonds in determining, for example, the secondary structure of proteins. The upper half of Table 7 lists the largest (>1 Hz) J couplings to O6 calculated for the two molecules. The calculated $^{2h}J_{ON}$ couplings of 5.3 and 5.7 Hz are of similar magnitude to the $^{2h}J_{ON}$ coupling constant of 11.3 Hz calculated using the EOM–CCSD method for the eight-atom HCNH$^+$···OC model complex, which also exhibits N–H···O hydrogen bonding.[21] Importantly, in the context of the potential for experimental determination, these results show that the $^{2h}J_{ON}$ couplings are of comparable magnitude to their $^{2h}J_{NN}$ counterparts. The O–N hydrogen-bond distances (2.837 and 2.841 Å) are very similar, and this is reflected in the small difference between $^{2h}J_{O_{6a}N_{2b}}$ and $^{2h}J_{O_{6b}N_{2a}}$; it should be noted that the N–H···O bond angles of 158.7 and 156.6 are similar and that both deviate from the ideal value of 180°, as do the N–H···N hydrogen bonds (Table 3). The $^{2h}J_{ON}$ couplings are positive, as expected for an X–H···Y hydrogen bond in which the magnetogyric ratios of X and Y have the same sign (^{15}N and ^{17}O both have negative magnetogyric ratios).[21,24]

In addition, the $^1J_{O_6C_1}$ couplings are calculated to be 22 Hz. Recently, the experimental solid-state NMR determination of values as small as 14 Hz for $^2J_{AlP}$ couplings involving ^{27}Al, which is also an $I = {}^5/_2$ nucleus, has been reported.[76] It is thus reasonable to expect that the $^{2h}J_{O_6N_1}$ and $^1J_{O_6C_1}$ couplings are large enough to be determined experimentally, though this will require the preparation of a sample with additional ^{17}O (and

(73) Bryce, D. L.; Eichele, K.; Wasylishen, R. E. *Inorg. Chem.* **2003**, *42*, 5085–5096.
(74) Hung, I.; Wong, A.; Howes, A. P.; Anupõld, T.; Pasat, J.; Samoson, A.; Mo, X.; Wu, G.; Smith, M. E.; Brown, S. P.; Dupree, R. *J. Magn. Reson.* **2007**, *188*, 246–259.
(75) Iuga, D.; Morais, C.; Gan, Z.; Neuville, D.; Cormier, L.; Massiot, D. *J. Am. Chem. Soc.* **2005**, *127*, 11540–11541.
(76) Amoureux, J. P.; Trébosc, J.; Wiench, J. W.; Massiot, D.; Pruski, M. *Solid State Nucl. Magn. Reson.* **2005**, *27*, 228–232.

Table 8. Calculated Solid-State $^{15}N-^{13}C$ J Couplings (Hz) for **3**[a]

molecule a	calcd value	molecule b	calcd value
$^1J_{N_{1a}C_{6a}}$	−12.3	$^1J_{N_{1b}C_{6b}}$	−12.3
$^1J_{N_{1a}C_{2a}}$	−12.7	$^1J_{N_{1b}C_{2b}}$	−12.3
$^2J_{N_{1a}C_{5a}}$	−6.9	$^2J_{N_{1b}C_{5b}}$	−6.7
$^1J_{N_{2a}C_{2a}}$	−24.9	$^1J_{N_{2b}C_{2b}}$	−24.6
$^3J_{N_{2a}C_{4a}}$	−3.2	$^3J_{N_{2b}C_{4b}}$	−3.2
$^1J_{N_{3a}C_{2a}}$	−8.4	$^1J_{N_{3b}C_{2b}}$	−6.0
$^1J_{N_{3a}C_{4a}}$	−10.1	$^1J_{N_{3b}C_{4b}}$	−8.3
$^2J_{N_{3a}C_{5a}}$	−1.2	$^2J_{N_{3b}C_{5b}}$	−1.7
$^2J_{N_{7a}C_{6a}}$	−5.8	$^2J_{N_{7b}C_{6b}}$	−5.8
$^1J_{N_{7a}C_{5a}}$	−2.4	$^1J_{N_{7b}C_{5b}}$	−3.2
$^1J_{N_{7a}C_{8a}}$	−2.3	$^1J_{N_{7b}C_{8b}}$	−1.9
$^1J_{N_{9a}C_{2a}}$	−3.8	$^1J_{N_{9b}C_{2b}}$	−3.6
$^1J_{N_{9a}C_{4a}}$	−18.4	$^1J_{N_{9b}C_{4b}}$	−18.5
$^1J_{N_{9a}C_{5a}}$	−7.5	$^1J_{N_{9b}C_{5b}}$	−7.5
$^1J_{N_{9a}C_{8a}}$	−12.9	$^1J_{N_{9b}C_{8b}}$	−12.5
$^1J_{N_{9a}C_{1'a}}$	−10.6	$^1J_{N_{9b}C_{1'b}}$	−10.8

[a] The labels a and b denote the two distinct molecules of **3** in the crystallographic unit cell and refer to molecules 1 and 2, respectively, in ref 52.

^{13}C) labeling (the samples used in refs 36 and 43 were ^{15}N-labeled only).

The lower half of Table 7 lists the calculated intramolecular $^{15}N-^{15}N$ couplings (>1 Hz) that were not included in Table 4. As noted above, a DQ correlation corresponding to the intramolecular $^2J_{NN}$ coupling between N_1 and N_2 was observed in the refocused INADEQUATE spectrum presented in ref 43. However, it was not possible to determine the $^2J_{N_1N_2}$ couplings from the spin-echo MAS data presented in ref 36 because of the fast dephasing (short T_2') observed for the protonated N_1 and N_2 resonances. We note that the calculated $^2J_{N_1N_2}$ couplings of 2.3 and 2.4 Hz are consistent with the $^2J_{N_1N_2}$ coupling of 2.2 Hz determined by solution-state NMR of guanosine-3′-phosphate.[77] Our calculations show that the two remaining two-bond intramolecular J couplings not considered so far, namely, $^2J_{N_1N_3}$ and $^2J_{N_7N_9}$, are the smallest in magnitude (1.1 to 1.3 Hz). Interestingly, weak intensity is evident in the DQ projection of the refocused INADEQUATE spectrum presented in ref 43 at the DQ frequency of −350 ppm corresponding to the $^2J_{N_7N_9}$ coupling.

Table 8 lists the calculated (>1 Hz) $^{15}N-^{13}C$ solid-state J couplings for **3**. The experimental determination of these $^{15}N-^{13}C$ J couplings would require the preparation of an ^{15}N- and ^{13}C-labeled sample. We note that the calculated $^1J_{CN}$ couplings are of the same magnitude as those determined by Trébosc et al.[78] for L-[U-^{13}C,^{15}N]histidine·HCl ($^1J_{CN} = 10-15$ Hz for the ring and 5.5 Hz for the $C_\alpha-$N bond). Experimental[79] and calculated[80] J_{CN} coupling constants for pyridine and pyridinium have revealed that for $^1J_{CN}$ in pyridine, the para-magnetic spin−orbit term is significant and of opposite sign to the Fermi-contact term, leading to a small calculated $^1J_{CN}$ value of 0.5 Hz (compared with calculated $^2J_{CN}$ and $^3J_{CN}$ values of 3.0 and −3.9 Hz, respectively). In contrast, $^1J_{CN}$ in the pyridinium ion was calculated to be −14.6 Hz.

4. Conclusions

We have demonstrated the flexibility and accuracy of our newly developed approach to calculating J coupling in the solid state. Specifically, we have shown the importance of correctly accounting for long-range electrostatic interactions in solid-state systems; it should be noted that our inherently solid-state method uses the crystal periodicity, i.e., there is no requirement to construct an appropriate cluster of individual molecules. We have used the calculations to investigate the nature of intramolecular hydrogen bonding in 6-aminofulvene-1-aldimines, correctly reproducing the differences in solution and solid-state values and also successfully distinguishing the differences in J coupling in pyrrole and triazole derivatives. We have also applied our approach to calculate intermolecular hydrogen-bond-mediated J couplings in guanosine ribbons; our calculation considered two dimers and thus 192 atoms, far exceeding the system size studied in previous quantum-chemical investigations. We confirmed the assignment of the measured J couplings, where an increase in $^{2h}J_{NN}$ is correlated with a decrease in the N−H···N hydrogen-bond distance, and also showed that the calculated $^{2h}J_{ON}$ couplings for the N−H···O hydrogen bonds are of similar magnitude to the $^{2h}J_{NN}$ couplings, suggesting that their experimental determination and utilization should be feasible.

We emphasize the great advantage of comparing experiment and calculation in the solid state as opposed to the established approach of comparing solution-state experiment with gas-phase (vacuum) calculations: there is no complication from solvent effects and hence no need to consider solvent effects in the calculations.

The development of computational approaches for the calculation of NMR chemical shifts in periodic solid-state systems[58,81,82] has been widely applied and has provided structural insight in a wide variety of applications.[83−96] We

(77) Buchner, P.; Maurer, W.; Ruterjans, H. *J. Magn. Reson.* **1978**, *29*, 45–63.

(78) Trébosc, J.; Amoureux, J. P.; Delevoye, L.; Wiench, J. W.; Pruski, M. *Solid State Sci.* **2004**, *6*, 1089–1095.

(79) Berger S., Braun S., Kalinowski, H.-O. *NMR Spectroscopy of the Non-Metallic Elements*; Wiley: Chichester, U.K., 1996.

(80) Del Bene, J. E.; Elguero, J. *Magn. Reson. Chem.* **2006**, *44*, 784–789.

(81) Sebastiani, D.; Parrinello, M. *J. Phys. Chem. A* **2001**, *105*, 1951–1958.

(82) Yates, J. R.; Pickard, C. J.; Mauri, F. *Phys. Rev. B* **2007**, *76*, 024401.

(83) Profeta, M.; Mauri, F.; Pickard, C. J. *J. Am. Chem. Soc.* **2003**, *125*, 541–548.

(84) Farnan, I.; Balan, E.; Pickard, C. J.; Mauri, F. *Am. Mineral.* **2003**, *88*, 1663–1667.

(85) Profeta, M.; Benoit, M.; Mauri, F.; Pickard, C. J. *J. Am. Chem. Soc.* **2004**, *126*, 12628–12635.

(86) Charpentier, T.; Ispas, S.; Profeta, M.; Mauri, F.; Pickard, C. J. *J. Phys. Chem. B* **2004**, *108*, 4147–4161.

(87) Hoffmann, A.; Sebastiani, D.; Sugiono, E.; Yun, S.; Kim, K. S.; Spiess, H. W.; Schnell, I. *Chem. Phys. Lett.* **2004**, *388*, 164–169.

(88) Yates, J. R.; Pickard, C. J.; Payne, M. C.; Dupree, R.; Profeta, M.; Mauri, F. *J. Phys. Chem. A* **2004**, *108*, 6032–6037.

(89) Benoit, M.; Profeta, M.; Mauri, F.; Pickard, C. J.; Tuckerman, M. E. *J. Phys. Chem. B* **2005**, *109*, 6052–6060.

(90) Yates, J. R.; Pham, T. N.; Pickard, C. J.; Mauri, F.; Amado, A. M.; Gil, A. M.; Brown, S. P. *J. Am. Chem. Soc.* **2005**, *127*, 10216–10220.

(91) Yates, J. R.; Dobbins, S. E.; Pickard, C. J.; Mauri, F.; Ghi, P. Y.; Harris, R. K. *Phys. Chem. Chem. Phys.* **2005**, *7*, 1402–1407.

(92) Ashbrook, S. E.; Le Polles, L.; Gautier, R.; Pickard, C. J.; Walton, R. I. *Phys. Chem. Chem. Phys.* **2006**, *8*, 3423–3431.

(93) Pickard, C. J.; Salager, E.; Pintacuda, G.; Elena, B.; Emsley, L. *J. Am. Chem. Soc.* **2007**, *129*, 8932–8933.

(94) Zurek, E.; Pickard, C. J.; Autschbach, J. *J. Am. Chem. Soc.* **2007**, *129*, 4430–4439.

(95) Ashbrook, S. E.; Berry, A. J.; Frost, D. J.; Gregorovic, A.; Pickard, C. J.; Readman, J. E.; Wimperis, S. *J. Am. Chem. Soc.* **2007**, *129*, 13213–13224.

(96) Uldry, A.-C.; Griffin, J. M.; Yates, J. R.; Perez-Torralba, M.; Santa Maria, M. D.; Webber, A. L.; Beaumont, M. L. L.; Samoson, A.; Claramunt, R. M.; Pickard, C. J.; Brown, S. P. *J. Am. Chem. Soc.* **2008**, *130*, 945–954.

envisage that the method employed here for the calculation of solid-state NMR *J* couplings will also find widespread application.

Supporting Information Available: Further computational details and calculated *J* couplings, complete ref 33, Cartesian coordinates and total energies of isolated **1** and **2**, and total energies and PDB files for geometry-optimized crystal structures. This material is available free of charge via the Internet at http://pubs.acs.org.

JA800419M